ELSEVIER

Polymer 40 (1999) 2271–2279

polymer

Dielectric study of dynamics of subchains and distribution of normal mode relaxation times in dilute and semidilute solutions of miscible block copolymers

Keiichiro Adachi[a]*, Hitotsugu Hirano[a], Juan J. Freire[b]

[a]*Department of Macromolecular Science, Graduate School of Science, Osaka University, Toyonaka, Osaka 560, Japan*
[b]*Departamento de Quimica Fisica, Facultad de Quimica, Universidad Complutense, 28040 Madrid, Spain*

Received 3 March 1998; accepted 2 June 1998

Abstract

We report on the dielectric normal mode relaxation of the isoprene block chains in dilute and semidilute solutions of butadiene–isoprene (BI) diblock copolymers and butadiene–isoprene–butadiene (BIB) triblock copolymers. The dielectric loss ε'' curves in dilute solutions with a concentration close to the overlapping concentration C^* agreed approximately with those predicted by the bead–spring model. Above a concentration about three times higher than C^*, the ε'' curves broadened with increasing concentration indicating the strong concentration dependence of the distribution of the normal modes. Two maxima of the ε'' curves were observed for BIB solutions. In semidilute solutions of BIB, the ε'' peak located in the high frequency side shifted little with concentration but the ε'' peak in the low frequency side shifted towards low frequency with increasing concentration. This suggests that the lower order normal modes are affected by entanglement effects but the higher order modes are not, for semidilute solutions. We have attempted to explain the distribution of the normal modes in terms of the blob model.

Keywords: Dielectric relaxation; Normal mode; Block copolymer

1. Introduction

The bead–spring model [1,2] has been a successful theory of molecular dynanics for isolated chains in dilute solution. In semidilute solutions, the molecular motions slow down as a result of entanglements and are approximately described by the tube model [3–5]. In studies of dielectric normal mode relaxation of type-A chains [6,7], such as polyisoprene and poly(ε-caprolactone), it was found that the distribution of the relaxation times in semidilute solution broadens with increasing concentration [8–10]. This behaviour cannot be explained by the tube model [3–5] because it predicts the same distribution of relaxation times as the Rouse theory [1]. The broadening of the distribution of relaxation times was also observed in our computer simulation of the dynamics in many chain systems [11,12]. The issue of the mode distribution in semidilute solution has not been settled yet, neither experimentally nor theoretically.

The dielectric relaxation spectrum of a type-A homopolymer is of the wedge-type and the intensity of the higher order modes is weak. In order to observe better the higher order normal modes, one may use block copolymers composed of miscible type-A and non-type-A polymers in which the intensity of the higher order modes is enhanced. Examples of such block copolymers are butadiene–isoprene (BI) diblock copolymers and butadiene–isoprene–butadiene (BIB) triblock copolymers in which the I-block chain belongs to type-A but the B-block chain does not. Usually block copolymers exhibit microphase structures. However, polyisoprene (PI) and polybutadiene (PB) are miscible even in the bulk state when their molecular weights are less than 50 000. Therefore, they are expected to be perfectly miscible in dilute and semidilute solutions in a common good solvent and hence the dynamics of the end and the middle part of the chains can be observed on BI and BIB, respectively. As will be seen in the theoretical discussion below, the intensity of the higher order modes becomes prominent on decreasing the size of the subchain.

Based on this view, we had already studied the dielectric behaviour of BI and BIB in bulk and concentrated solution

* Corresponding author.

0032-3861/99/$ - see front matter
PII: S0032-3861(98)00450-9

[13]. The study was extended to dilute and semidilute solutions and the preliminary results were reported briefly [14]. It was found that the dielectric loss curves in dilute solutions of BI and BIB agree approximately with the Rouse theory [1], but in the range above the overlapping concentration, C^*, the loss curves broaden strongly with concentration [14]. In the present study, we report on the dielectric behaviour of solutions of BI and BIB in more detail. We firstly compare the experimental data in dilute solution with previous work [1,2] and then observe how the distribution of relaxation times varies with concentration. We also compare the behaviour of BI and BIB with the behaviour in solutions of homo-PI [8,9].

2. Theory

2.1. Dielectric normal mode relaxation of subchain

Let us consider a random flight chain composed of $N+1$ repeat units numbered 0 to N from the one end to the other. The coordinate of the jth unit is R_j and the mean bond length is b. The time-autocorrelation function $\phi(t)$ of the vector $\mathbf{r}_{mn} = \mathbf{R}_m - \mathbf{R}_n$ is defined by

$$\phi(t) = \frac{\langle \mathbf{r}_{mn}(0) \cdot \mathbf{r}_{mn}(t) \rangle}{\langle r_{mn}^2 \rangle} \tag{1}$$

The normalized complex dielectric constant $\varepsilon^*/\Delta\varepsilon$ is given by the Fourier transform of the correlation function $\phi(t)$:

$$\frac{\varepsilon^* - \varepsilon_\infty}{\Delta\varepsilon} = \int_0^\infty -\frac{\mathrm{d}\phi}{\mathrm{d}t} \exp(-i\omega t)\, \mathrm{d}t \tag{2}$$

where ε_∞ is the high frequency dielectric constant, $\Delta\varepsilon$ the relaxation strength, and ω the angular frequency. The relaxation strength $\Delta\varepsilon$ is given by [7,9]

$$\frac{\Delta\varepsilon}{C_{nm}} = \frac{4\pi N_A \mu^2 \langle r_{nm}^2 \rangle}{3 k_B T M_{nm}} \tag{3}$$

where μ is the dipole moment per unit contour length of the type-A subchain, N_A is the Avogadro number, C_{mn} is the concentration of the subchain (in g/cm^3), $\langle r_{nm}^2 \rangle$ is the the mean square distance between the nth and mth beads ($=(m-n)b^2$), and M_{nm} is the molecular weight of the block.

2.2. Bead–spring model

The dielectric normal mode relaxation in dilute solution is described by the bead–spring model as follows [1,2]. The random flight chain considered above is replaced by a chain consisting of N springs and $N+1$ beads. Among these beads, the beads with the indices n to m have parallel type-A dipoles. Then, the theoretical ε^* is written as:

$$\frac{\varepsilon^* - \varepsilon_\infty}{\Delta\varepsilon} = \sum_p \frac{g_p}{1 + i\omega\tau_p} \tag{4}$$

where g_p and τ_p are the intensity and the relaxation time, respectively, of the pth normal mode. According to the free-draining Rouse model, g_p and τ_p of the pth mode are given by [1,5,7]

$$g_p = \frac{8N}{(m-n)\pi^2} \frac{1}{p^2} \sin^2\left(\frac{p\pi(n+m)}{2N}\right) \sin^2\left(\frac{p\pi(m-n)}{2N}\right) \tag{5}$$

$$\tau_p = \frac{\zeta N \langle r^2 \rangle}{3\pi^2 k_B T p^2} \tag{6}$$

where ζ is the friction coefficient per bead and $\langle r^2 \rangle$ is the mean square end-to-end distance. For the non-draining Zimm model, g_p is given by Eq. (5) but τ_p is given by

$$\tau_p = \frac{\pi^{3/2} \eta_s b^3 N^{3/2}}{12^{1/2} \lambda_p k_B T} \tag{7}$$

where η_s is the solvent viscosity and λ_p is the eigenvalue of the pth mode [15].

2.3. Blob model

The tube model [3–5] predicts that g_p is given by Eq. (5) and τ_p is given by the same form as Eq. (6), i.e. $\tau_p = \tau_D/p^2$. Here τ_D is the longest relaxation time τ_1 of the tube model. The difference between the Rouse theory and the reptation theory is in the expression of τ_1. Therefore, both theories predict exactly the same distribution of the relaxation times.

De Gennes [16,17] assumed that a chain in semidilute solution is composed of N_b blobs and that it is confined in a tube with the diameter being equal to the correlation length ξ. N_b is given by

$$N_b = \left(\frac{C}{C^*}\right)^{1/(3\nu - 1)} \tag{8}$$

where C is the concentration of the chains and C^* is the overlapping concentration. The length of the tube L is ξ times the number of blobs N_b.

Here we assume a semidilute solution of chains composed of $N+1$ beads and N springs. Each blob contains $z = N/N_b$ beads. The beads are located inside of the blob move according to the bead–spring model but the overall chain moves according to the tube model. In other words, the Rouse–Zimm modes with the indices $p > N_b$ are not affected by entanglement but the relaxation times for the modes for $p < N_b$ are prolonged on account of entanglement. De Gennes proposed two blob models [16,17]. In the non-draining blob model, solvent molecules cannot go through the blob and hence the friction is proportional to the diameter of the blob as given by the Stokes law. In the free-draining model, the friction is proportional to the number of beads contained in the blob. The non-draining

blob model predicts that the relaxation time τ_p with $p < N_b$ is given by [17]

$$\tau_p = \frac{\tau_1^0}{p^2}\left(\frac{C}{C^*}\right)^{3(1-\nu)/(3\nu-1)} \quad (9)$$

where τ_1^0 is the relaxation time for the first normal mode and ν is the Flory exponent characterizing the molecular weight dependence of the chain dimension. On the other hand, the free-draining blob model predicts that [16]

$$\tau_p = \frac{\tau_1^0}{p^2}\left(\frac{C}{C^*}\right)^{2(1-\nu)/(3\nu-1)} \quad (10)$$

It was indicated that τ_p given by Eq. (10) corresponds to the relaxation time reduced to an iso-monomeric friction state [8].

Muthukumar and Freed [18,19] proposed a theory to represent the concentration dependence of τ_p around C^*:

$$\tau_p = \tau_p^0(1 + CAp^{-\kappa} - \sqrt{2}(CAp^{-\kappa})^{1.5} + 2(CAp^{-\kappa})^{2.0} - \ldots) \quad (11)$$

where τ_p^0 is the relaxation time in dilute solution, A is a constant proportional to the intrinsic viscosity, and κ is equal to $3\nu - 1$.

3. Experimental

3.1. Samples

BI and BIB block copolymers were prepared by anionic polymerization with sec-butyllithium in *n*-heptane at about 20°C. The weight and number average molecular weight, M_w and M_n, were determined with a gel permeation chromatograph (GPC; Tosoh HLC 801A) equipped with a low angle light-scattering photometer (Tosoh LS-8000). The characteristics of the samples are summarized in Table 1 where the code number indicates the block molecular weight in 10 kg/mol. Solvents *n*-hexane (C6) and *n*-hexadecene (C16) of high purity grade were from Dojin Chemicals. *n*-Hexane was used as received. To avoid crystallization of *n*-hexadecene, we mixed it with decaline (10 wt%). Hereafter C16 means a mixed solvent of *n*-hexadecene/decaline (9/1 w/w). Polymer concentration C, in units of g/cm^3, was determined from the densities of solutions estimated by assuming the additivity of densities ρ of the components: $\rho = 0.66$, 0.79, 0.89, and 0.91 for C6, C16, PB, and PI, respectively.

3.2. Measurements

Dielectric measurements were carried out at 273 and 303 K with a transformer bridge (General Radio 1615A) and an LCR meter (Hewlett-Packard 4284A) in the frequency range 20 Hz–500 kHz. To increase the accuracy of measurements, we used a condenser cell with an empty capacitance of 130 pF. Details of measurements were reported previously [9].

Intrinsic viscosity $[\eta]$ was measured with a capillary viscometer of Ubbelohde-type. The solvent viscosity was also determined by the same viscometer.

3.3. Reduced molecular weight and overlapping concentration

In order to compare the dielectric data with theory it is required to reduce the molecular weight M(B) and the monomeric friction coefficient ζ_o of the PB block chain to those equivalent to PI. Since the characteristic ratios C_∞ for PI and PB were reported to be similar [20], the reduced molecular weight of PB, M_r(B), is simply given by $M_r(B) = M(B)M_o(I)/M_o(B)$ where M_o(I) and M_o(B) are the molecular weights of the isoprene and butadiene unit, respectively. The reduced molecular weights thus calculated are listed in Table 1. We also assume that the monomeric friction coefficients of PI and PB in dilute and semidilute solutions are the same, since the structures of the two types of monomers are similar, as discussed previously [13]. In the case of BIB with the block molecular weights of M(B1), M(I), and M(B2), n and m appearing in Eq. (5) are calculated in such a way that $n = M_r(B1)/M_r(total)$ and $m = [M_r(B1) + M(I)]/M_r(total)$ where M_r(total) is the reduced molecular weight of the whole BIB molecule.

Table 1
Weight average molecular weight M_w of B1, I, and B2 blocks, reduced molecular weight of B1 and B2 blocks[a] and the overlapping concentration C^*[b]

Code	M_w(B1)	M_w(I)	M_w(B2)	M_r(B1)	M_r(B2)	M_r	10^2C^*
BI(8-3)	7.6	3.1	–	9.6	–	12.7	1.30
BI(20-8)	20.4	8.2	–	25.7	–	33.9	0.69
BI(66-24)	66.2	23.6	–	83.4	–	107.0	0.33
BIB(8-3-8)	7.6	3.1	7.6	9.6	9.6	22.3	0.90
BIB(20-8-24)	20.4	8.2	24.3	25.7	30.6	64.5	0.45
BIB(66-24-41)	66.2	23.6	41.2	83.4	51.7	158.7	0.25

[a]The unit of molecular weight is 10 kg/mol. The polydispersity factor M_w/M_n is less than 1.1 and typically 1.05. The microstructures (in mol%) of *cis*-PI blocks and that of PB blocks prepared in this study are expected to be similar to those of homo-PI and PB prepared by anionic polymerization in heptane and are reported previously [12].
[b]In g/cm^3.

The overlapping concentration C^* (=1/[η]) was determined as follows. Urakawa et al. [9] reported that the exponents of the Mark–Houwink–Sakurada equation of PI and PB in heptane are 0.638 and 0.634, respectively. Since heptane has similar solvent quality to C6 and C16, C^* of BI and BIB was estimated with $C^* = KM_r^{-0.64}$ where K (=27.2) was determined from the average value of [η] of BIB(8-3-8) in C6 ([η] = 103) and that in C16 ([η] = 118 g^{-1} cm^3). The values of C^* thus estimated are listed in Table 1.

4. Results and discussion

4.1. Frequency dependence of dielectric loss

Figs 1–3 show the representative double logarithmic plots of dielectric loss factor ε'' divided by polymer concentration C (in g/cm^3) versus frequency f for solutions of BI(66-24), BIB(8-3-8), and BIB(20-8-24), respectively. In each figure, the ε''/C curves of C6 and C16 solutions at 303 K are compared. The dielectric constants ε' are not shown since our capacitance bridge was not sufficiently sensitive to detect low dielectric dispersions of the order of 10^{-4}. Since the relaxation frequency of the loss peaks seen in Figs 1–3 is much lower than the relaxation frequency for segmental motions (10 MHz–10 GHz), they are assigned to the normal mode relaxation.

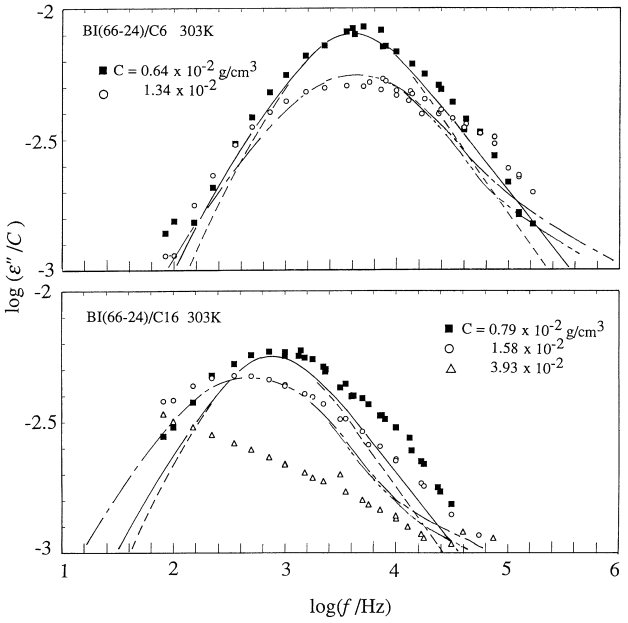

Fig. 1. Double logarithmic plot of dielectric loss factor ε'' divided by polymer concentration C versus frequency f for hexane (C6) and hexadecene (C16) solutions of BI(66-24). The values of C of the BI are given in the figure. Solid and dashed lines indicate the theoretical curves calculated with the Rouse and Zimm models, respectively. Dash-dot and dash-dot-dot lines represent the curves calculated with the model-2 with a = 0.14 and 0, respectively (see Eq. (14)).

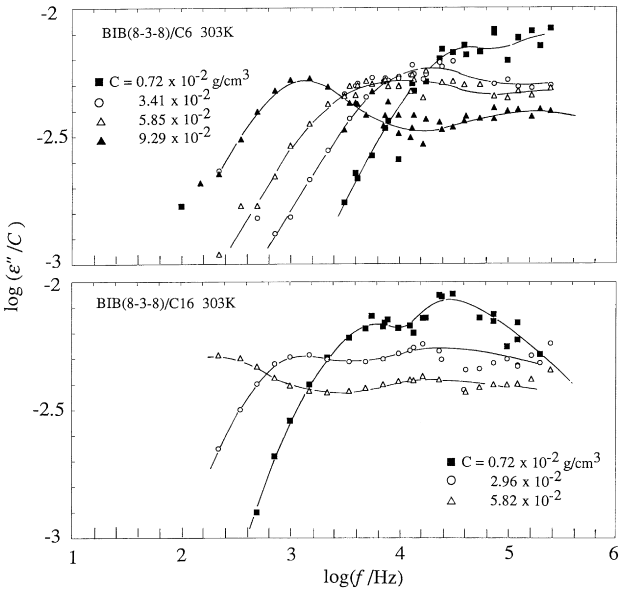

Fig. 2. Double logarithmic plot of dielectric loss factor ε'' divided by concentration C versus frequency f for hexane (C6) and hexadecene (C16) solutions of BIB(8-3-8). The concentrations C of the BIB are given in the figure. Solid lines are a guide for the eye.

As is seen in Figs 1–3, BI solutions exhibit a single ε'' peak while BIB solutions exhibit a bimodal ε'' curve. The ε''/C curves for BI and BIB indicate the difference of dynamics between the end and the middle parts of the chains. As usual the nominal relaxation time τ_n is defined by $\tau_n = 1/(2\pi f_{max})$, where f_{max} is the loss maximum frequency. It is noted that the theoretical τ_n calculated with the Rouse model for homo-PI is very close to the longest relaxation time τ_1 but τ_n/τ_1 for block copolymers depends strongly on the architecture.

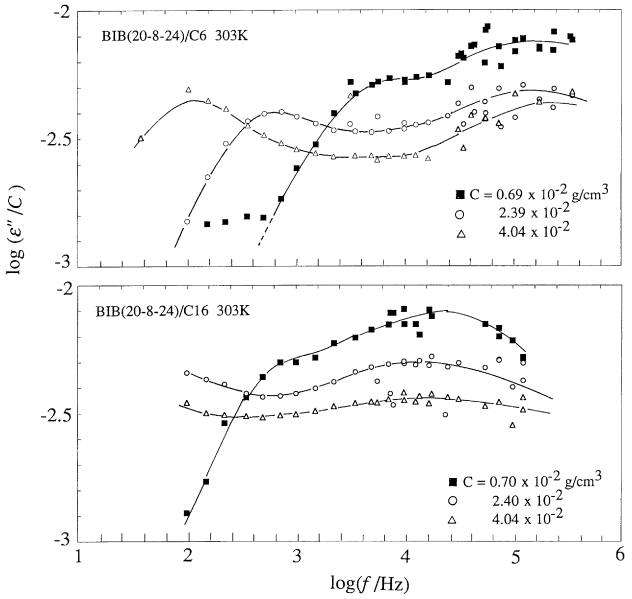

Fig. 3. Double logarithmic plot of dielectric loss factor ε'' divided by concentration C versus frequency f for hexane (C6) and hexadecene (C16) solutions of BIB(20-8-24). Solid lines are a guide for the eye.

4.2. Superposition of ε'' curves of C6 and C16 solutions

In Figs 1–3, we see that the shape of the ε'' curve for C6 solutions is approximately the same as that of C16 solutions at the same C. This indicates that $\varepsilon''(f)$ of C6 solution can be superposed with $\varepsilon''(a_\eta f)$ of the C16 solution. Here a_η is the shift factor and is about 8 indicating that the relaxation time of the chains is proportional to the solvent viscosity η_s as given by the Rouse–Zimm theories [1,2]. Specifically, η_s of C6 and C16 at 303 K are 0.286 and 2.31 centipoise, respectively.

In the superposition of the ε'' curves of C6 and C16 solutions, it is required to check the solvent qualities of C6 and C16 for BI or BIB. If they are largely different, the mode distribution of BI or BIB in C6 and C16 could be different due to the excluded volume effect and then the ε'' curves of C6 and C16 might not be superposable. In order to assess the ratio of the solvent qualities of C6 and C16, we measured the intrinsic viscosities of BIB(8-3-8) in C6 and C16 to be 103 and 118 g^{-1} cm^3, respectively. The close $[\eta]$ values in both solvents ensure that the qualities of C6 and C16 against BI and BIB are approximately the same.

The master curves of log ε''/C versus log f of solutions of BIB(8-3-8) and BIB(20-8-24) were constructed by shifting the ε'' curves along the log f axis by log $[\eta(C16)/\eta(C6)]$. Here η denotes the solvent viscosity of C16 and C6. The results are shown in Figs 4 and 5. For BI solutions we did not construct the master curves since the whole ε'' curves are given in Fig. 1.

4.3. Dilute solution

4.3.1. Relaxation spectra in dilute solution

The theoretical relaxation spectra g_p and the ε'' curves for BI and BIB samples are calculated with Eqs. (4)–(6). Representative examples of g_p/g_{pm} and corresponding $\varepsilon''/\varepsilon''_m$ are shown in Fig. 6 for PI, BI(66-24), and BIB(20-8-24) where the subscript m indicates the maximum. It is noted that log (g_p/g_{pm}) is plotted against log (τ_1/τ) so that the g_p and ε'' curves can be compared directly.

It is instructive to see the relationship between the intensity and the normal coordinate. In the insets of Fig. 6,

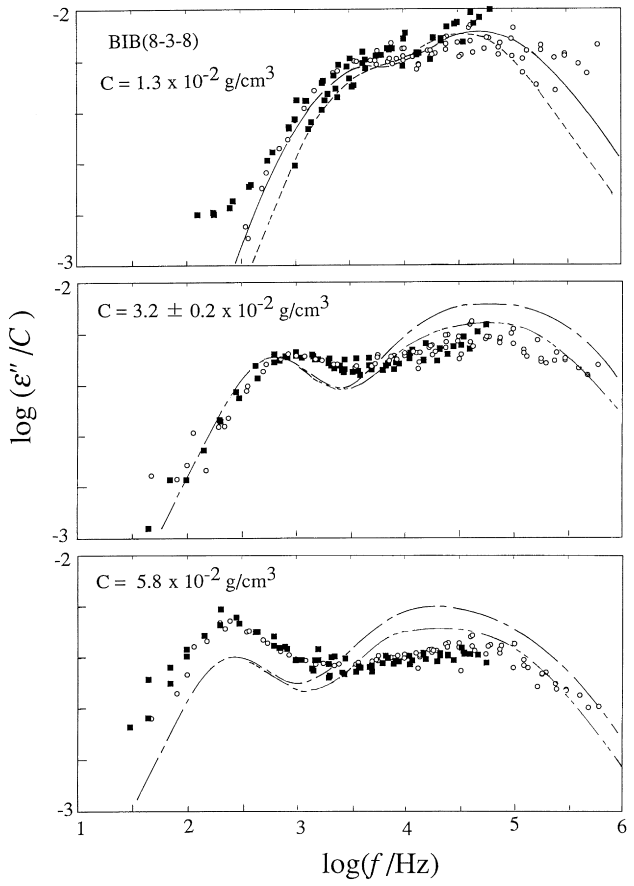

Fig. 4. Master curve of dielectric loss factor ε'' divided by concentration C constructed from the data for hexane (C6) (■) and hexadecene (C16) (○) solutions of BIB(8-3-8). Solid and dashed lines indicate the theoretical curves calculated with the Rouse and Zimm models, respectively. Dash-dot and dash-dot-dot lines are calculated with the model-2 with $a = 0.14$ and $a = 0$, respectively.

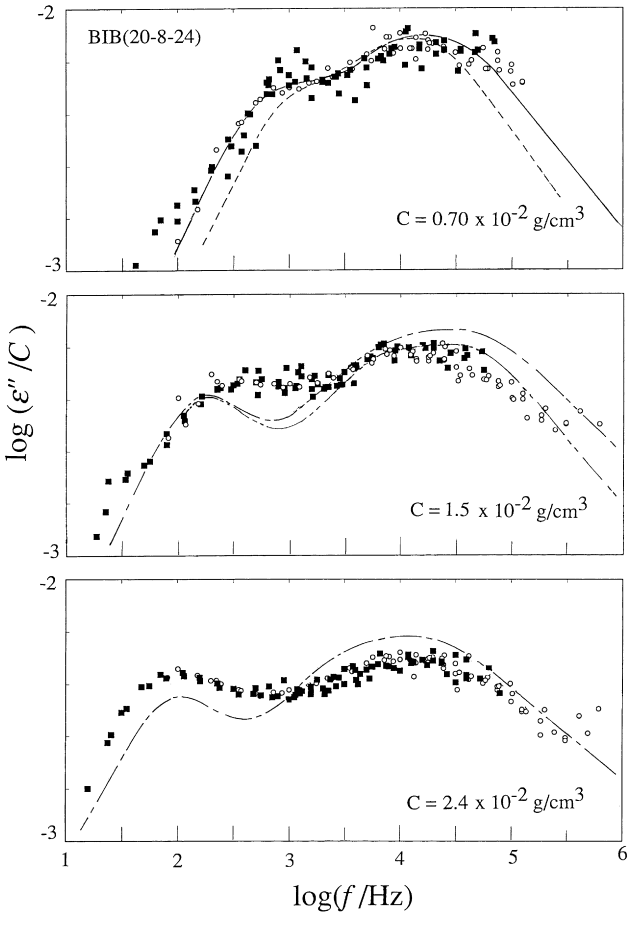

Fig. 5. Master curve of dielectric loss factor ε'' divided by concentration C constructed from the data for hexane (C6) (■) and hexadecene (C16) (○) solutions of BIB(20-8-24). Solid and dashed lines indicate the theoretical curves calculated with the Rouse and Zimm models, respectively. Dash-dot and dash-dot-dot lines are calculated with the model-2 with $a = 0.14$ and $a = 0$, respectively.

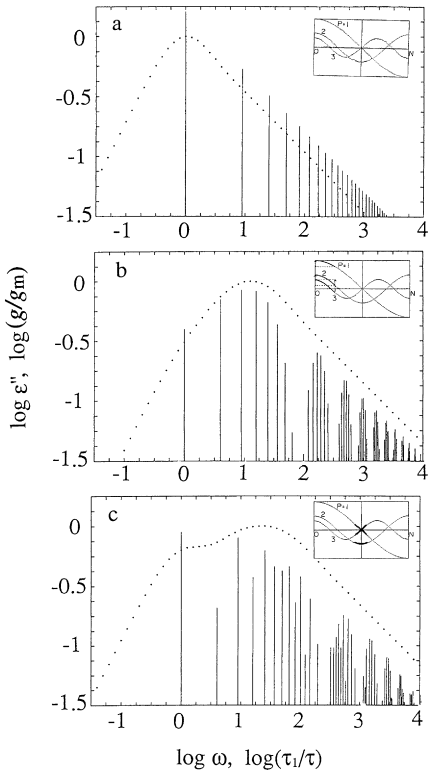

Fig. 6. Theoretical curves of log ε'' versus log ω (dotted lines) and log $g(\tau)$ versus log (τ_1/τ) (histograms) calculated with the Rouse theory for (a) PI, (b) BI(66-24), and (c) BIB(20-8-24). The insets indicate the first three normal modes and the amplitude of the oscillation of dipoles indicated by the thick lines.

the normal coordinates for $p = 1$, 2, and 3 are depicted. The mode oscillates as a standing wave. In a homo type-A chain in which $n = 0$ and $m/N = 1$, only the odd number modes are dielectrically active since the even number modes do not induce a change of dipole moment. The spectrum is of a wedge-type as shown in Fig. 6(a).

For BI(66-24), the beads from $n = 0$ to $m/N = 0.24$ are labelled with the dipoles as indicated in the inset of Fig. 6(b) by the thick solid line but the other beads are non-polar. It is seen that when these modes oscillate, the dipole vectors change their orientation with the amplitude as indicated by the arrows. We note that the amplitude for the third mode is the largest as reflected in the g_p versus τ spectrum. The shape of the spectrum changes sensitively with m/N. For BIB, only the beads located in the middle of the chain are labelled by the type-A dipole. The modes with $p = 1$, 2 and 3 are also illustrated in the inset of Fig. 6(c). It is seen that the first and third modes cause the oscillation of the dipole moment of the I block and their amplitudes are similar. The second mode does not contribute if the I block locates exactly at the middle of the chain. In BIB(20-8-24) the second mode contributes a little due to the slight asymmetry. As shown in Fig. 6(c), g_p values of $p = 4$–10 have similar intensities to the third mode. Thus the ε'' curve becomes bimodal: the low frequency peak is mainly due to the overall motion of the BIB molecule (the mode of $p = 1$) and the high frequency peak to the oscillation of the subchain in the middle part.

4.3.2. Comparison of observed and theoretical ε'' curves

In Figs 1, 4 and 5, the theoretical ε'' curves calculated on the basis of the Zimm theory (dashed line) and the Rouse theory (solid line) are compared with the observed ε'' curves at the lowest concentrations. It is desirable to compare the ε'' curves at $C \ll C^*$ with the theories. Unfortunately the lowest concentration used in the present study was around the overlapping concentration C^* $(=1/[\eta])$ where intermolecular interactions are not negligible. For example, C^* of BI(66-24) solution is 0.0033 g/cm^3 but the lowest concentration used in our experiment for BI(66-24) was 0.007 g/cm^3 for C6 solution and 0.008 g/cm^3 for C16 solution.

As seen in Figs 1, 4 and 5, the observed ε'' curves at $C \approx C^*$ are slightly broader than the theoretical loss curve calculated with the Zimm theory and close to the Rouse theory. As pointed out frequently [21,22], the dynamical properties agree with the Rouse model rather than the Zimm theory in the crossover region and are described by the reptation theory above the entanglement concentration C_e $(\approx 3C^*)$. It is expected that at sufficiently low concentration the experiment agrees with the Zimm theory. In fact, the ε'' curves of homo-PIs and homo-poly(lactone)s [9] in dilute solution agreed with the Zimm theory [2]. To summarize, the dielectric behaviour of BI and BIB around $C \approx C^*$ agrees fairly well with the Rouse model within experimental error.

Finally we should consider the effect of the difference in the monomeric friction coefficients between the isoprene and butadiene blocks. The effect was already discussed by using the Stockmayer–Kennedy theory [23] in Ref. [16] and it was concluded that the effect is small in the case of BI and BIB.

4.4. Semidilute solution

4.4.1. Muthukumar–Freed model

The ε'' curves for homo-type-A chains ($n = 0$ and $m = N$) at various C/C^* are calculated with the Mutjukumar–Freed theory (Eqs. (5), (7) and (10)) and shown in Fig. 7. It is seen that with increasing C/C^* the theoretical ε'' curve exhibits a

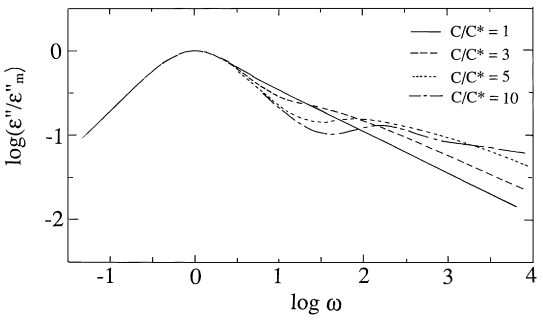

Fig. 7. Normalized ε'' curves of a type-A chain calculated by the Muthukumar–Freed theory for the case of $n = 0$ and $m/N = 1$ and at C/C^* given in the figure.

hollow. This behaviour has never been observed experimentally in homo-PI solutions [7–10]. Due to this disagreement we will not use the Muthukumar–Freed theory to explain the C/C^* dependence of the ε'' curves of BI and BIB solutions. Probably, the exact calculation of higher order terms of Eq. (10) is needed to compare the theory with the experiment.

4.4.2. Blob model

For fully entangled chains, the reptation model [3–5] predicts that g_p is given by Eq. (5) and τ_p is given by τ_D/p^2. Here τ_D denotes the longest relaxation time (τ_1) of the tube model (tube disengagement time). Thus the dielectric relaxation spectrum is exactly the same as the Rouse model. As seen above, the dielectric loss curve broadens with increasing C for semidilute solutions. Obviously the simple view that the Rouse model is switched to the reptation model as C exceeds C^* cannot explain the experimental results. Adachi et al. [14] attempted to explain the broadening based on the Ngai theory [24]. There it was necessary to assume that the coupling increased with increasing mode number, which is inconsistent with the Ngai theory.

We analyse the relaxation spectrum $g(\tau)$ based on the blob model [16,17]. Fig. 8 shows schematically the $\log g(\tau)$ versus $\log \tau$ curve for a BIB chain. In Fig. 8(a) the curve illustrated by the solid line indicates $g(\tau)$ for the isolated state ($N_b = 1$) and the dashed lines for the fully entangled state ($N_b \gg 1$). The shapes are the same as mentioned above.

In the state where N_b is finite, the blob model leads us to expect that the slow modes with $p < N_b$ are governed by the reptation model. Then the relaxation times of the pth modes are expected to increase with concentration as $\tau_p \approx \tau_1^0 N_b^{k(1-\nu)}/p^2$, while the fast modes with $p > N_b$ conform to the Rouse theory: $\tau_p \approx \tau_1^0/p^2$. Here $k = 3$ for the non-draining model (Eq. (9)) and k = 2 for the free-draining model (Eq. (10)). Thus $g(\tau)$ splits into two regions as depicted in Fig. 8(b). Hereafter this model is referred to as 'model-1'.

The model-1 is qualitatively supported by the observation. As is seen in Figs 2 and 3, the location of the high frequency peak of the ε' curve around $\log f = 4$ does not change with increasing C but the low frequency peak shifts rapidly to lower frequency with C. Fig. 9 shows $\log(\tau_L/\tau_H)$ for BIB(8-3-8) and BIB(20-8-24) solutions plotted against $\log(C/C^*)$, where τ_L and τ_H represent the nominal relaxation times for the low and high frequency peaks, respectively. If we assume that τ_H is independent of C, Eqs. (9) and (10) predict the slopes 2.07 and 1.08, respectively, with $\nu = 0.55$. The former agrees with the observed slope of 2.0 of the $\log(\tau_L/\tau_H)$ versus $\log(C/C^*)$ plot.

However, the model-1 predicts that the relaxation spectrum has a wide gap in the spectrum when C is higher than C^*. This is not in accordance with the experiments because the ε'' curves of homo-type-A chains calculated with the model-1 exhibit a hollow. Thus the model-1 does not agree with our experiments.

4.4.3. A modified blob model

In the above sections we see that both the Muthukumar–Freed theory and the blob model cannot explain the observed mode distribution. Now we seek an empirical relaxation spectrum which is required to satisfy the three conditions: (1) τ_1 is given by the tube model, (2) the modes with $p < N_b$ are given by the Rouse model, and (3) there is no wide gap in the spectrum between the modes of $p = N_b$ and $p = N_b - 1$.

Based on these requirements, we assume a relaxation spectrum in which the modes of $p < N_b$ have a p-dependence different from the p^{-2} proportionality: $\tau_p/\tau_1 = p^{-\beta}$. Furthermore, we assume that the spectrum in the region of $p < N_b$ (Fig. 8(b)) is stretched along the abscissa so that the whole spectrum does not have a wide gap in the spectrum

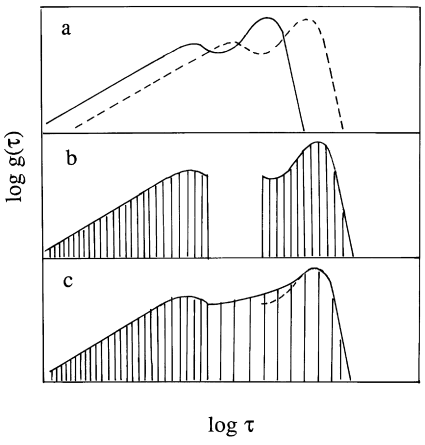

Fig. 8. Schematic relaxation spectra $g(\tau)$ for a BIB chain: (a) $g(\tau)$ of free (solid line) and entangled (dashed line) states; (b) $g(\tau)$ predicted by the model-1; (c) $g(\tau)$ predicted by the model-2.

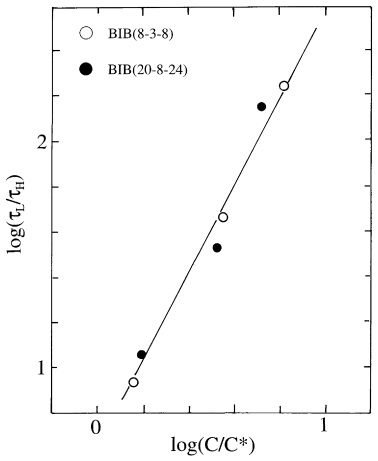

Fig. 9. Log (τ_L/τ_H) for BIB(8-3-8) and BIB(20-8-24) solutions plotted against log (C/C^*) where τ_L and τ_H represent the nominal relaxation times for the low and high frequency peaks, respectively.

as depicted in Fig. 8(c). Since the non-draining blob model (Eq. (9)) predicts that $\tau_1 \approx \tau_1^0 N_b^{3(1-\nu)}$, we obtain $\tau_p \approx \tau_1^0 N_b^{3(1-\nu)}/p^\beta$ for the modes with $p < N_b$. On the other hand, Eq. (6) gives $\tau_p \approx \tau_1^0/p^2$ for $p > N_b$. At $p = N_b$, the former and the latter become equal. Thus β becomes $5 - 3\nu$. If we assume the free-draining blob model (Eq. (10)), we obtain $\beta = 4 - 2\nu$. Since $\nu = 0.55$ for the present system, β becomes 3.35 for the non-draining model and 2.90 for the free-draining model. For the sake of simplicity, we assume $\beta = 3.0$. Thus the mode distribution given by the model-1 is modified as

$$\tau_p = \frac{\tau_1^0 N_b}{p^3} \quad (p < N_b) \tag{12}$$

$$\tau_p = \frac{\tau_1^0}{p^2} \quad (p > N_b) \tag{13}$$

This model is referred to as 'model-2'. It is noted that the present rough model would not hold for fully entangled systems.

Urakawa et al. [25,26] reported experimentally that the ratio of τ_1/τ_2 in semidilute solutions of a bifurcated polyisoprene was close to 4. This result indicates that at least τ_p values of $p = 1$ and 2 obey the tube model. Since the present analysis is semi-quantitative and also for the sake of simplicity, we adopt the model-2 given above.

So far we have modified the p-dependence of τ_p. We should also introduce an alternative modification for the description of the intensity g_p of the pth mode. Freire et al. studied the computer simulation of chain dynamics in many chain systems in terms of the Monte Carlo (MC) method [27–30]. It was found that the time-correlation function of the end-to-end vector of homopolymers are consistently described if g_p is given by

$$g_p = p^a g_p(\text{Rouse}) \tag{14}$$

where a was found to be approximately 0.14 and g_p(Rouse) is the theoretical intensity given by Eq. (5). Details are described elsewhere [12]. Eq. (14) also helps to reach a slightly better description of the experimental ε'' curves for the homopolymer chains.

4.5. Comparison of the model with experiments

Firstly we examine the model-2 for homo-PI solutions. The ε'' curves of semidilute solutions of homo-PI broaden with concentration in the high frequency side of the ε'' peak and the log ε'' versus log f curves are linear in the frequency range $\log f > \log f_m + 1$:

$$\log\varepsilon''(\omega) = -\alpha\log\omega + \text{const.} \tag{15}$$

Fig. 10 shows the normalized ε'' curves for a homo-PI with $M_w = 743\,000$ in heptane [9], i.e. ε'' divided by the maximum loss ε''_m is plotted against f/f_m. In the range $C \gg C^*$, the exponent α converges to 0.27 ± 0.03 which is smaller than 0.5 predicted by the tube theory.

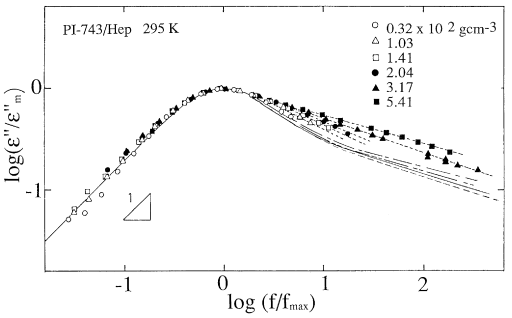

Fig. 10. Normalized ε'' curves of solutions of PI-743 with $M_w = 743\,000$ in heptane at 295 K. C^* is 0.004 g/cm^3. The solid line indicates the Zimm theory. The dash-dot and dash-dot-dot lines indicate the curves calculated with the model-2 with $a = 0.14$ at $C/C^* = 1.41$ and 3.17, respectively. The solid and dashed lines are those with $a = 0$ at $C/C^* = 1.41$ and 3.17, respectively.

We calculated the $\varepsilon''/\varepsilon''_m$ curves for the model-2 with and without taking Eq. (14) into account. In Fig. 10 the solid and dashed lines indicate the $\varepsilon''/\varepsilon''_m$ curves calculated with $a = 0$ at $C = 0.0141$ ($C/C^* = 4.7$) and $C = 0.0317$ ($C/C^* = 7.9$), respectively. The dash-dot and dash-dot-dot lines are those with $a = 0.14$ at $C = 0.0141$ ($C/C^* = 4.7$) and $C = 0.0317$ ($C/C^* = 7.9$), respectively. As is seen in this figure the slope α of the theoretical curve in the high frequency range is close to that of the experimental curve. The shape of the overall curve also agrees fairly well. However, we note that the intensities of the modes of $p = 1$ and 3 for the theoretical curves are too strong to explain the experiments. Consequently it can be observed that introducing $a = 0.14$ in Eq. (14) gives a slightly better description of the experimental data than $a = 0$. Recently Watanabe et al. [26,31] explained the broad dielectric relaxation spectrum of bulk PI with non-sinusoidal normal modes. Such analyses would also explain the present results.

The theoretical ε'' curves corresponding to BI(66-24) are calculated at $C = 0.0134$ and $C = 0.0158$ with the model-2 and plotted in Fig. 1 by the dash-dot lines for $a = 0.14$ and the dash-dot-dot line for $a = 0$. It is seen that the theoretical curve is slightly narrower than the observed curves and the effect of Eq. (14) is not appreciable.

In Figs 4 and 5, we test the model-2 for BIB solutions. It is seen that the theoretical curves agree approximately with the experimental curves. However, the intensity around the high frequency peak is higher than the observed ε''. For the copolymer cases the modified model with $a = 0$ describes slightly better the high frequency region than by assuming $a = 0.14$. This is the reverse trend to the case of homo-PI. The discrepancy may be explained by taking into account the excluded volume effect.

In our previous paper we reported that the I-block chain in BIB is expanded [13]. If we take into account this effect, the effective chain length of the middle part becomes longer than the length calculated with Eq. (3) and hence the n and m values of Eq. (3) should be changed since the effective chain length of the I block becomes longer than

the unperturbed state. To see the effect of expansion of the middle part, the theoretical ε'' curves of symmetrical BIBs are calculated with the Rouse model in which the fraction of the middle part $(m - n)/N$ is changed from 10 to 30%. We found that the slight increase of the value of $(m - n)/N$ causes a substantial decrease of the ratio of the heights of the low and high frequency peaks. Thus the excluded volume effect is one of the origins of the discrepancies of the intensities of ε'' curves.

5. Conclusions

We have studied the dielectric normal mode relaxation of BI and BIB in dilute and semidilute solutions. The dielectric loss ε'' versus frequency f curves of BI and BIB in dilute solutions with concentration $C \approx C^*$ agree with the Rouse theory. In the range $C > 3C^*$, the ε'' curves become broader with increasing C. The ε'' curve of BIB is bimodal. The nominal relaxation times τ for the high (H) and low (L) frequency sides indicate that τ_H is almost independent of C but τ_L increases with C for semidilute solutions. The ratio τ_L/τ_H is proportional to $C^{2.1}$ in agreement with the non-draining blob theory. In order to explain the broadening of the loss curves with increasing C, we have proposed a modified blob model in which the pth relaxation time τ_p is proportional to p^{-3} in the range of p less than the number of blobs N_b. The model explains semi-quantitatively the dielectric data.

Acknowledgements

J.J.F. thanks the Japan Society for the Promotion of Science for the JSPS fellowship in 1995, and also the partial support by the Grant PB95-0384 from the DGICYT.

References

[1] Rouse PE. J Chem Phys 1953;21:1272.
[2] Zimm BH. J Chem Phys 1956;24:269.
[3] De Gennes PG. J Chem Phys 1971;55:572.
[4] Doi M, Edwards SF. J Chem Soc Faraday Trans 2 1978;74:1789.
[5] Doi M, Edwards SF. Theory of polymer dynamics. Oxford: Clarendon Press, 1986.
[6] Stockmayer WH. Pure Appl Chem 1967;15:539.
[7] Adachi K, Kotaka T. Progr Polym Sci 1993;18:585.
[8] Adachi K, Kotaka T. Macromolecules 1988;21:157.
[9] Urakawa O, Adachi, K, Kotaka T. Macromolecules 1993;26:2036, 2042; Macromolecules 1994;27:7410.
[10] Patel SS, Takahashi KM. Macromolecules 1992;25:4382.
[11] Freire JJ, Adachi K. Macromolecules 1995;28:4747.
[12] Freire JJ, Molina LA, Rey A, Adachi K. in preparation.
[13] Adachi K, Nishi I, Doi H, Kotaka T. Macromolecules 1991;24:5843.
[14] Adachi K, Hirano H, Kotaka T. J Non-Cryst Solids (Vol. 172–174) 1994:661.
[15] Zimm BH, Roe GR, Epstein LF. J Chem Phys 1956;24:279.
[16] de Gennes P-G. Macromolecules 1976;9:587–594.
[17] de Gennes P-G. Scaling concept in polymer physics. Ithaca, NY: Cornell University Press, 1979.
[18] Muthukumar M, Freed KF. Macromolecules 1978;11:843.
[19] Muthukumar M. Macromolecules 1984;17:971.
[20] Mark JE. J Am Chem Soc 1966;88:4353.
[21] Adachi K, Kotaka T. J Molecular Liq 1987;36:75.
[22] Takahashi Y, Isono Y, Noda I. Macromolecules 1985;18:1002.
[23] Stockmayer WH, Kennedy JW. Macromolecules 1975;8:351.
[24] Ngai KL, Rendell R, Rajakopal AK, Teitler S. Ann NY Acad Sci 1986;484:150.
[25] Urakawa O. Doctoral thesis, Osaka University, 1994.
[26] Watanabe H, Yamada H, Urakawa O. Macromolecules 1995;28: 6443.
[27] Lopez Rodriguez A, Rey L, Freire JJ. Macromolecules 1992;25:3266.
[28] Rubio AM, Freire JJ, Bishop M, Clarke JHR. Macromolecules 1993;26:4018.
[29] Lopez Rodriguez A, Freire JJ. Macromolecules 1991;24:3578.
[30] Rey A, Freire JJ, Garcia de la Torre J. J Chem Phys 1989;90:2035.
[31] Watanabe H, Yao ML, Osaki K. Macromolecules 1996;29:97.